

**PREPARATION, MODELING, AND OPTIMIZATION OF MECHANICAL PROPERTIES OF EPOXY/HIPS/SILICA HYBRID NANOCOMPOSITE USING COMBINATION OF CENTRAL COMPOSITE DESIGN AND GENETIC ALGORITHM.
PART 1. STUDY OF DAMPING AND TENSILE STRENGTHS**

Y. Rostamiyan¹ and A. B. Fereidoon

UDC 539.4

Brittle nature and poor resistance in front of vibrational waves despite of good mechanical strength have limited widespread use of epoxy resins in industry. In current study a new combination of thermoplastic and particulate nanofiller is used as modifier to enhance simultaneously tensile strengths and damping properties in first and second modes of epoxy-based nanocomposite. High impact polystyrene (HIPS) as thermoplastic phase and silica nanoparticles as particulate phases incorporately used to obtain ternary epoxy-based nanocomposite. In current study solution blending as dispersion mechanism is used to prepare homogenous mixture and brings good molecular level of mixing. Tensile and damping properties in first and second modes were the two different mechanical tests investigated in order to achieve higher toughness strengths without attenuating desired mechanical properties. Also central composite design is employed to present mathematical models for predict mechanical behaviors of epoxy/HIPS/silica nanocomposite as function of physical factors. The effective parameters investigated were HIPS, SiO₂, and hardener contents. Based on mathematical functions obtained from central composite design model, the genetic algorithm as one of powerful optimization tools is applied to find optimum values of mentioned mechanical properties. From the results it can be found that combination of HIPS and silica nanoparticles significantly increased tensile and damping strengths of epoxy resin up to 69, 42, and 91%, respectively. The morphology of fracture surface is also studied by scanning electron microscopy.

Keywords: epoxy, toughness, high impact polystyrene, silica, tensile, damping, central composite design, genetic algorithm, scanning electron microscope.

Introduction. Epoxy polymer is one of the most applicable thermoset matrices used for reinforced composite materials, due to its high elastic modulus, considerable rupture strength, low creep and good performance at elevated temperature[1–3]. Despite the above improved characteristics, epoxy materials have a brittle nature, low toughness, and poor damping characteristics[4]. Blending of various kinds of thermoplastic polymers [5, 6] or microphase dispersed rubber [7–9] has been a conventional way to increase impact strength of epoxy matrices for many years. In applications of rubber and thermoplastic phases aimed at improval of impact strength, in view of dramatic effects on other mechanical properties, quite popular is the material toughening by engineering thermoplastic, such as polysulfone [10], polyether amide [11], ABS [12], and polyethersulfone [13]. Although, in many cases, presence of elastomeric phase in epoxy matrix enhances toughness and, consequently, damping properties, but on the other hand, it provides an increase in viscosity and drastic reduction of strength, elastic modulus and stiffness [14–17]. In the last years, one of the well-known proposed ways to increase the material stiffness implied usage of rigid inorganic particles with glass or ceramic base, having diameter between 4 to 100 μm [18, 19], but due to large size of these particles, the viscosity of the epoxy resin was also increased, which made the product processing quite problematic

Semnan University, Semnan, Iran (¹y.rostamiyan@yahoo.com). Translated from Problemy Prochnosti, No. 5, pp. 146 – 165, September – October, 2013. Original article submitted December 14, 2012.

[20]. In the last decade, application of nanophase structures in polymer matrices, in order to improve mechanical properties, such as tensile, compressive and flexural strengths, have opened new horizons, in comparison with conventional composite materials [20]. Usage of nanoparticles such as silica, resulted in no considerable viscosity enhancement, due to their small sizes [21]. The distinction between nano- and microparticles is mainly due to their high specific surface (relation of the surface to the mass) [22–24]. Previous studies have shown that addition of relatively cost-effective nanosilica into epoxy matrix can considerably improve the mechanical strength [20, 25]. It is noteworthy that addition of nanoparticles may strongly affect the mechanical strength, but has no considerable effect on impact strength improvement of epoxy-based composites [26]. Also some studies have shown that usage of both soft particles, and rigid fillers in epoxy resin as a hybrid composite, may enhance simultaneously the strength and toughness. For instance, adding micron-sized glass spheres, including rubber particles, into epoxy matrices has shown a synergistic toughening effect with acceptable strength enhancement [27, 28]. In order to study the mechanical properties and hybrid mechanism of epoxy-based nanocomposite, the effective quantitative factors must be introduced. Conventionally, based on numerous studies [29–31], it can be found that the weight percentage of reinforcement such as toughening agent and nanofiller is the most critical parameter, which controls the mechanical behavior of epoxy-based nanocomposites. Another important factor in epoxy/thermoplastic/nanoparticle sample preparation is the weight percentage of hardener. Although determination of appropriate value of this factor is based on stoichiometric ratio, one can expect that presence of thermoplastic phase as toughening agent, as well as of nanofiller in epoxy resin, would dramatically reduce the probability of complete mixture of epoxy monomers and hardener, and hence hinder the complete polymerization. Mirmohseni and Zavareh [12] have determined the optimum amount of hardener according to the maximum tensile and impact strengths of the prepared epoxy samples. This type of optimization is called OVAT (one variable at a time) [32]. Leardi [32] concluded in his research that 93% of scientific publications on optimization, development, and improvement of these materials was based on the OVAT model. Due to the fact that in many approaches the optimized variables are interrelated with each other, these interrelations need to be determined, but the OVAT model cannot guarantee that the real optimum point is reached [32]. Moreover, prediction of the nonlinear effect of each parameter requires availability of at least three experimental points as parameter levels, which increases the number of required experiments for model prediction and, consequently, increases the costs. The central composite design (CCD), which was introduced by Box and Wilson [33], is one of very useful types of sequential second-order experimental design, which provides simultaneous reduction of the number of experiments, predicts a probable nonlinear effect of each parameter, as well as interrelations of coupled parameters. Within framework of the mathematical model, one of optimization methods should be used to predict the optimum values. Based on the famous research of Charles Darwin, genetic algorithm has been applied as a powerful tool for solving complex problems [34]. Many researchers used this method for optimization of numerous case studies in engineering [34–36]. Genetic algorithm is a global optimization method, which codes the design variables by individual genes or chromosomes [35]. The result based on this algorithm has feeble associations with the original problem. This method can find the answer to a wide range of problems and can govern a large number of responses at the same time. This feature reduces the possibility that the algorithm is being trapped in the local optimum points. This algorithm is easily applied for solving problems that have a large number of variables. Moreover, the genetic algorithm is simple, needs no auxiliary information like derivative of the objective function, and can be used for optimization of intricate objective functions, discontinuous or non-differentiable function or systems which have no specific mathematical definition [34].

In the current work, addition of the combination of thermoplastic (HIPS) and particulate nanofiller (silica) to epoxy matrix is provided, in order to ensure simultaneous improvement of tensile strength and damping characteristics. Central composite design is applied for elaboration of a model for predicting the mechanical behavior of the above nanocomposite. Based on the obtained mathematical function from CCD, the genetic algorithm is employed to find the optimum conditions. In addition, the authors tried to use inorganic nanofillers and commercial thermoplastic to reduce the total costs of sample preparation and concurrently achieve a considerable enhancement of the mechanical properties. Morphological and structural characteristics of the hybrid mechanism are investigated using scanning electron microscopy (SEM).

1. Experimental.

1.1. Materials. Epoxy resin utilized in current study was an undiluted clear difunctional bisphenol A, Epon 828 provided by Shell Chemicals Co. with epoxide equivalent weight 185–192 g/eq. Epon 828 is basically DGEBA (diglycidyl ether of bisphenol-A). The curing agent was a nominally cycloaliphatic polyamine, Aradur[®] 42 supplied by Huntsman Co. The spherical silica nanoparticles with average particle size 10–15 nm and SSA (specific surface area) 180–270 m²/g were supplied from TECNAN Ltd. The high impact polystyrene used in this study was purchased from Tabriz petrochemical Company in Iran. The solvent used was tetrahydrofuran (THF) with purity (GC) exceeding 99% provided by Merck Co (Germany).

1.2. Sample Preparation. In order to prepare a homogenous mixture, all of reinforcement-adding procedures into resin were conducted in a proper solvent. Solution blending is a liquid-state powder processing method that ensures a good molecular level of mixing and is widely used in material preparation and processing [25]. Some of the limitations of melt mixing can be overcome if both the polymer and the nanoparticles are dissolved or dispersed in solution and recovered after mixing. In order to avoid various solvents' effects, as well as to achieve the comparable results, the authors employed THF as an appropriate solvent for dissolving all mixture components such as epoxy resin, silica and, especially, high impact polystyrene. For preparing neat epoxy samples, in order to ensure equal conditions and comparability with other specimens, liquid epoxy resin was poured into adequate amount of THF solvent and after 30 min mixing by magnetic stirrer the mixture was poured into a vacuum flask and the solvent evaporated completely under vacuum conditions using the vacuum pump. At this step, the stoichiometry ratio of cycloaliphatic polyamine as hardener, i.e., 23 phr was added and mixed uniformly for 15 min and degassed by a vacuum pump to remove the air bubbles. The mixture was poured into silicon mould and cured for 24 h at room temperature, which was followed by post-curing from 50 to 90°C each 2 h at 20°C temperature enhancement interval and at 120°C for 2 h to ensure complete curing. In order to prepare epoxy/HIPS/SiO₂ samples, desired amount of the reinforcements was dissolved in adequate amount of mentioned solvent and mixed via magnetic stirrer for 30 min. In the current study, the mixture was homogenized by ultrasonic treatment (Ultrasonic SONOPULS-HD3200, 50% amplitude, 20 kHz, and pulsation; on for 10 s and off for 3 s) for 30 min. The required amount of epoxy resin with the same procedure as mentioned before was added to this mixture and mixed mechanically at high speed for 2.5 h, and subsequently the mixture was subjected to ultrasonic treatment by the same procedure for 30 min. The same protocol was used for the neat epoxy, whereas stoichiometric ratio of hardener content was varied for each hybrid sample.

1.3. Characterization. The tensile tests were conducted according to ASTM D638 at room temperature. This test method covers the determination of the tensile properties of reinforced plastics in the form of standard dumbbell-shaped test specimens. The dimensions of specimens were chosen according to the type I of this standard test method. The rate of motion of the driven grip when the testing machine was running was 5 mm/min. For each sample five specimens were tested. All of tensile tests are conducted via STM-150 universal testing machine from Santam Company (Iran) with load capacity 150 kN. For the specimens of damping test the authors used izod impact unnotched specimens according to ASTM D256 with the dimensions of 63.5, 12.7, and 7.2 mm as indicated in standard. The laser doppler vibrometer OMETRON VH300+, which is shown in Fig. 1, was used for measuring vibrations. In the current test, calculation of damping coefficients is based on stochastic subspace identification–data (SSI-data) method, which was introduced by Van Overschee and De Moor [37] and modified by Peeter and Brinker [38, 39]. Based on this method, the specimen was treated as cantilevered beam with environmental excitation. All time-dependent responses were accumulated in Block Henkel Matrix and converted into individual Past and Future matrices. At this step, in order to make connection between responses, the future matrix was projected at past matrix and created the projection matrix [37–39]. By severance singular value decomposition (SVD) of projection matrix, observability matrix and Kalman states are calculated, and the collection of polar system matrix is achieved. At this step, as it is shown in Fig. 2, in order to calculate damping coefficients and natural frequencies, the stabilization diagram is used. The stabilization diagram is a tool to show polars of systems of different order [33–35]. To display and analyze the measurement results on a workstation, the Polytec Vibrometer Software (VibSoft) was optionally used. A scanning electron microscope (SEM 1530) from TECNAN was utilized to observe the dispersion of fracture surfaces of the cured composites. The fracture surface was gold-coated prior to SEM studies, in order to avoid charging, and was examined at 15 kV accelerating voltage.



Fig. 1. Vibration measurement by laser doppler vibrometer OMETRON VH300+ (a) and specimen (b).

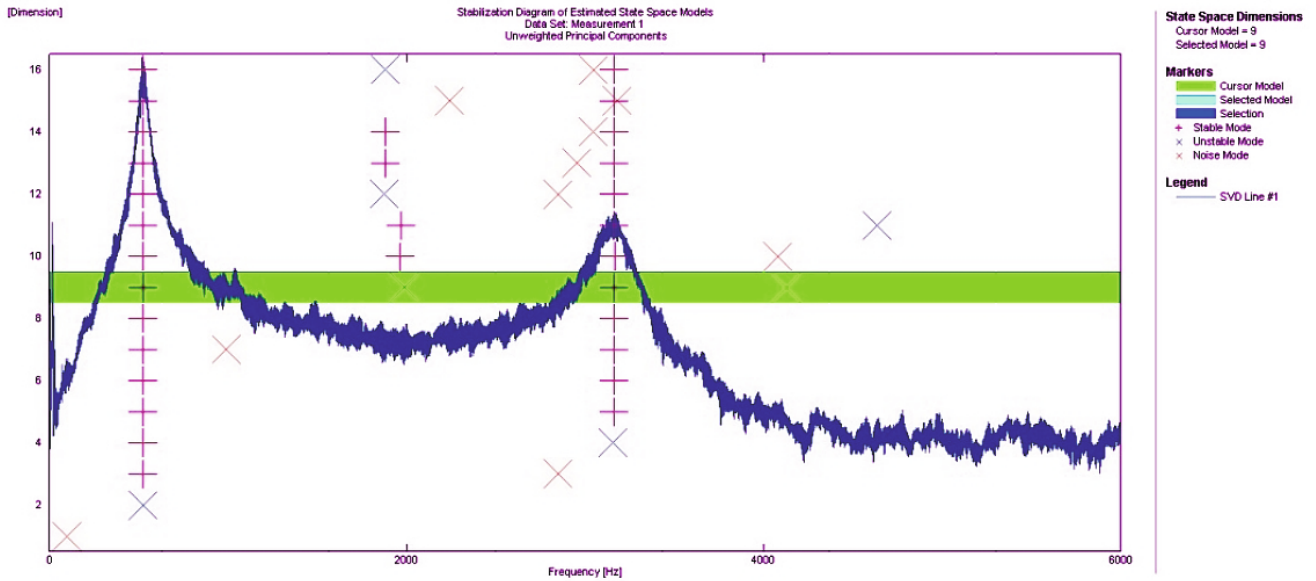


Fig. 2. Example of stabilization diagram in SSI-data method for neat epoxy.

1.4. Design of Experiment. In order to present the mathematical model, central composite design is used as one of the well-known experimental designs [40, 41]. Based on this type of design, N experiments should be executed for f factors, according to the following formulation:

$$N = N_f + N_a + N_0, \quad (1)$$

where $N_f = 2^f$ represents two-level full factorial points and $N_a = 2f$ corresponds to extra star points located at $\pm\alpha$ from the center of the experimental domain. Also N_0 is the number of experiments repeated at the center of the design carried out to provide an independent estimation of the “pure” experimental error variance. This value must be calculated by considering the rotatability and orthogonality of the design. If the variance of responses for all variables at distance α from the center of the experimental domain is constant, a design would be rotatable [40]. The required value α for rotatability is calculated via the following equation:

$$\alpha = \pm(N_f)^{1/4}. \quad (2)$$

The STATISTICA software as statistical package version 7.0 (Stat Soft Inc., Tulsa, USA) was used for experimental design analysis and data processing. In current study, the CCD is employed to predict models for

TABLE 1. Actual and Coded Levels of the Design Parameters

Factors	Levels			Star points $\alpha = 1.68179$	
	Low (-1)	Central (0)	High (+1)	$-\alpha$	$+\alpha$
(X_1) HIPS content (wt.%)	4.0	7.0	10.0	2	12
(X_2) SiO ₂ content (wt.%)	2.8	5.5	8.2	1	10
(X_3) hardener content (Phr)	23.0	26.0	29.0	21	13

TABLE 2. Experimental Design and Corresponding Responses

Run No.	Experimental factors (coded value)			Responses of mechanical tests		
	HIPS content	SiO ₂ content	Hardener content	Tensile strength (MPa)	First mode damping (%)	Second mode damping (%)
1 (C)	0	0	0	65 ± 4	3.49 ± 0.22	4.35 ± 0.13
2	-1.68179	0	0	68 ± 5	3.67 ± 0.09	4.33 ± 0.16
3	-1.00000	1.00000	1.00000	63 ± 2	3.69 ± 0.12	4.44 ± 0.08
4	1.00000	1.00000	1.00000	50 ± 3	3.35 ± 0.16	3.98 ± 0.05
5 (C)	0	0	0	62 ± 5	3.53 ± 0.04	4.42 ± 0.19
6	-1.00000	-1.00000	1.00000	68 ± 3	3.68 ± 0.07	4.52 ± 0.06
7	1.00000	1.00000	-1.00000	33 ± 4	2.47 ± 0.19	3.40 ± 0.24
8	0	0	-1.68179	52 ± 2	2.58 ± 0.24	3.79 ± 0.16
9	0	1.68179	0	43 ± 3	3.31 ± 0.16	4.18 ± 0.11
10	-1.00000	-1.00000	-1.00000	62 ± 1	3.28 ± 0.08	4.22 ± 0.09
11	1.00000	-1.00000	-1.00000	48 ± 4	2.56 ± 0.05	2.81 ± 0.18
12	0	-1.68179	0	64 ± 2	3.30 ± 0.15	3.75 ± 0.16
13	0	0	1.68179	66 ± 2	3.69 ± 0.26	4.54 ± 0.22
14	1.00000	-1.00000	1.00000	62 ± 1	3.40 ± 0.19	3.39 ± 0.15
15	1.68179	0	0	48 ± 5	2.64 ± 0.27	2.76 ± 0.12
16	-1.00000	1.00000	-1.00000	55 ± 4	2.98 ± 0.13	4.03 ± 0.21

Note. C is the central point.

tensile and damping properties of epoxy-based hybrid nanocomposite. The input variables investigated were HIPS, SiO₂ and hardener contents. Actual and coded levels of the design parameters are described in Table 1.

As shown in Table 2, 16 samples with different compositions for 3 factors with 2 replications at the center point have been designed. Noteworthy is that, in order to avoid random errors, all treatments were set in a random order. The responses obtained from mechanical tests including coded values are presented in Table 2. According to central composite design model, the result should be fit to the following basic second-order polynomial equation:

$$Y = b_0 + \sum_{i=1}^f b_i x_i + \sum_{i=1}^f b_{ii} x_i^2 + \sum_{i=1}^{f-1} \sum_{j=i+1}^f b_{ij} x_i x_j, \quad (3)$$

where b_0 is constant, b_i shows the linear effect of x_i , b_{ii} shows the quadratic nonlinear effect of x_i , and b_{ij} indicates the interaction between parameters. In central composite design the analysis of variance (ANOVA) is used to determine the significance of model terms. After elaboration of the mathematical model, different optimization algorithms can be used to optimize the results. In order to validate the optimized results, the optimum condition should be satisfied.

TABLE 3. Analysis of Variance for Central Composite Design Models

Function of response	Source of variation									Error	Total – SS	
	X_1	X_1^2	X_2	X_2^2	X_3	X_3^2	X_1X_2	X_1X_3	X_2X_3			
Y_1 (UTS)	Sum of square	575.265	46.828	404.421	136.554	344.035	33.258	28.125	36.125	3.125	26.188	1558.438
	Df ¹⁾	1	1	1	1	1	1	1	1	1	6	15
	Mean square	575.265	46.828	404.421	136.554	344.035	33.258	28.125	36.125	3.125	4.3647	–
	F-value ²⁾	131.7987	10.7288	92.6566	31.2858	78.8216	7.6198	6.4437	8.2766	0.7160	–	–
	P-value	0.000026	0.016918	0.000072	0.001389	0.000114	0.032837	0.044173	0.028172	0.429918	–	–
Y_2 (Damping at 1st mode)	Sum of square	0.939637	0.147666	0.012501	0.049665	1.615294	0.164670	0.002813	0.046512	0.015313	0.04110	2.893375
	Df	1	1	1	1	1	1	1	1	1	6	15
	Mean square	0.939637	0.147666	0.012501	0.049665	1.615294	0.164670	0.002813	0.046512	0.015313	0.00685	–
	F-value	137.1735	21.5570	1.8249	7.2503	235.8096	24.0394	0.4106	6.7902	2.2354	–	–
	P-value	0.000023	0.003530	0.225446	0.035926	0.000005	0.002703	0.545353	0.040347	0.185508	–	–
Y_3 (Damping at 2nd mode)	Sum of square	2.879001	0.833834	0.195305	0.212685	0.717978	0.060494	0.262812	0.025313	0.001512	0.006103	4.963644
	Df	1	1	1	1	1	1	1	1	1	6	15
	Mean square	2.879001	0.833834	0.195305	0.212685	0.717978	0.060494	0.262812	0.025313	0.001512	0.001017	–
	F-value	2830.382	819.752	192.006	209.093	705.853	59.472	258.374	24.885	1.487	–	–
	P-value	0	0	0.000009	0.000007	0	0.000249	0.000004	0.002481	0.268446	–	–

Note. ¹⁾ Degree of freedom. ²⁾ Test for comparing model variance with residual (error) variance.

2. Results and Discussion.

2.1. Statistical Modeling. As it was mentioned before, in order to reduce the number of experiments required for elaboration of the mathematical model and final optimization of the results, the CCD method was used, and the results of tensile and damping tests in the first and second modes were obtained and tabulated in Table 2. The important fact is that each treatment response was replicated five times, the average values being listed in Table 2. Using STATISTICA software for predicting responses, the following equations were proposed:

$$Y_1 = 63.626 - 6.490(X_1) - 2.248(X_1)^2 - 5.442(X_2) - 3.839(X_2)^2 + 5.019(X_3) - 1.895(X_3)^2 - 1.875(X_1X_2) + 2.125(X_1X_3) + 0.625(X_2X_3), \quad (4)$$

$$Y_2 = 3.51 - 0.26(X_1) - 0.126(X_1)^2 - 0.03(X_2) - 0.073(X_2)^2 + 0.344(X_3) - 0.133(X_3)^2 + 0.0187(X_1X_2) + 0.0762(X_1X_3) + 0.0437(X_2X_3), \quad (5)$$

$$Y_3 = 4.386 - 0.459(X_1) - 0.3(X_1)^2 + 0.119(X_2) - 0.151(X_2)^2 + 0.229(X_3) - 0.081(X_3)^2 + 0.181(X_1X_2) + 0.056(X_1X_3) + 0.0137(X_2X_3), \quad (6)$$

where Y_1 , Y_2 , and Y_3 correspond to the ultimate tensile strength (UTS), damping ratio at the first and second modes of epoxy-based ternary nanocomposite, respectively. At this stage, in order to demonstrate the effectiveness of each parameter, the ANOVA tables listed in Table 3 should be used. Based on the ANOVA results, the confidence level was determined at 95% and the significance of each parts of model was evaluated based on their probability (P -value). If the terms have a significant effect on response, the probability value will be less than 0.05 and the null hypothesis (H_0) will be rejected [40]. The terms having no significant effect (i.e., with P -value higher than 0.05) are eliminated from the final equation of the model. The final results that illustrate the effective or non-effective terms are presented in the form of Pareto charts and are shown in Fig. 3. After determining the effective terms, Eqs. (4)–(6) are reduced to the following forms:

$$\hat{Y}_1 = 63.626 - 6.490(X_1) - 2.248(X_1)^2 - 5.442(X_2) - 3.839(X_2)^2 + 5.019(X_3) - 1.895(X_3)^2 - 1.875(X_1X_2) + 2.125(X_1X_3), \quad (7)$$

$$\hat{Y}_2 = 3.51 - 0.26(X_1) - 0.126(X_1)^2 - 0.073(X_2)^2 + 0.344(X_3) - 0.133(X_3)^2 + 0.0762(X_1X_3), \quad (8)$$

$$\hat{Y}_3 = 4.386 - 0.459(X_1) - 0.3(X_1)^2 + 0.119(X_2) - 0.151(X_2)^2 + 0.229(X_3) - 0.081(X_3)^2 + 0.181(X_1X_2) + 0.056(X_1X_3). \quad (9)$$

Another criterion for evaluating the ability of the reduced model to predict results is coefficient of determination (R^2). When this value is close to 100%, the model provides an accurate estimate of the results. The value of (R^2) related to each model is shown in the predicted-observed diagram for each model in Fig. 4. Using STATISTICA software, the 3D and contour graphs related to mechanical behavior of nanocomposite depending on variable parameters were plotted in Figs. 5–7.

2.2. Optimization of the Mechanical Properties. In this study, one of the main goals is to optimize the effective factors to obtain the best content of new hybrid epoxy-based nanocomposite. One of the common techniques for achieving the optimum conditions within framework of the central composite design is usage of

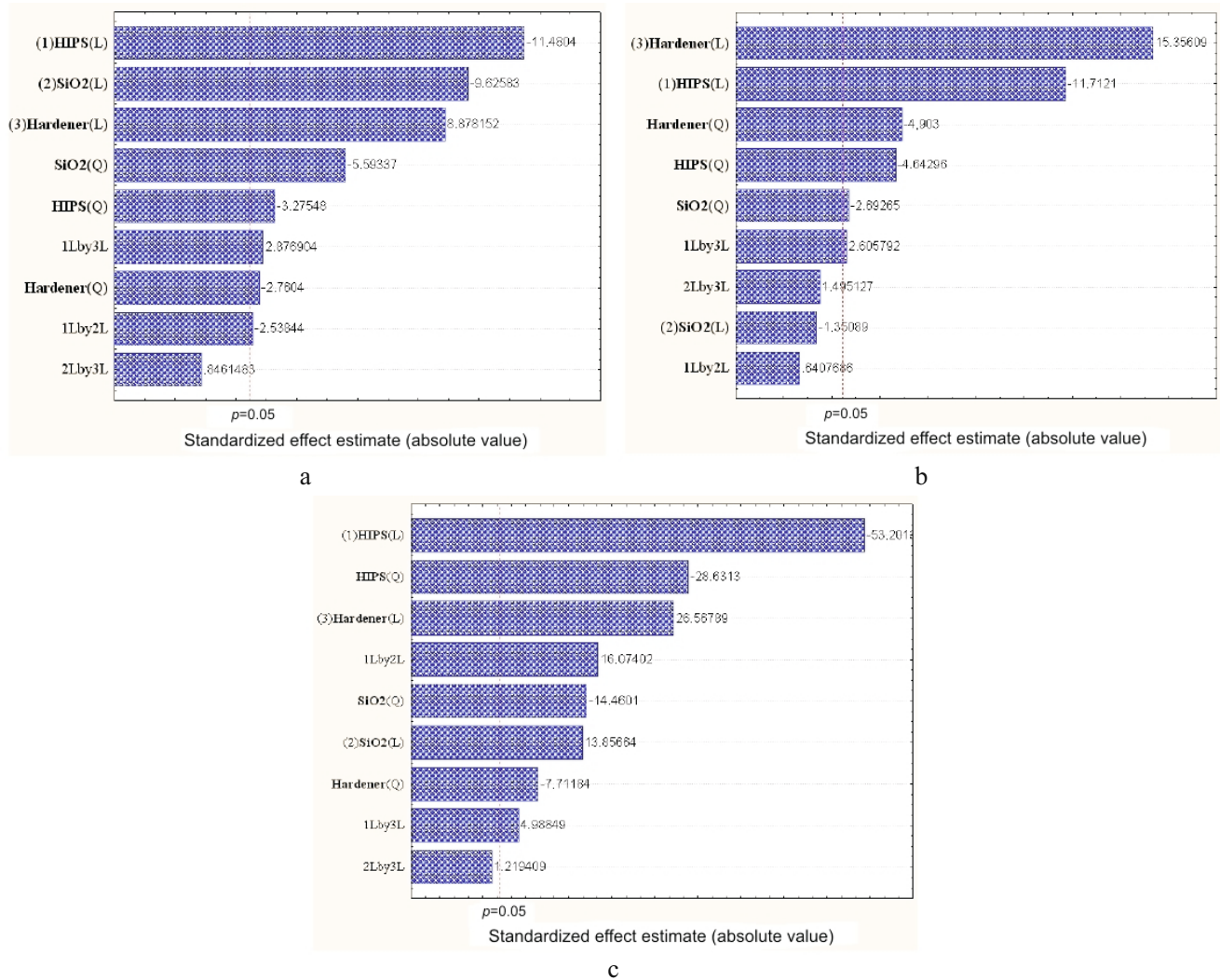


Fig. 3. Pareto chart of standardized effects: (a) tensile; (b) damping ratio-first mode; (c) damping ratio-second mode.

profiles for predicted values and desirability functions shown in Fig. 8, which are provided by STATISTICA software that can be a proper tool for controlling the behavior of each parameter and its effect on responses. But in this study, upon elaboration of the final mathematical model for each mechanical property, a genetic algorithm provided by Matlab software is used to find more accurate conditions on content instead of those provided by the desirability function. At first, genetic algorithm starts working with a population of chromosomes, which are randomly selected. In order to obtain a better generation, genetic operators are applied to the population. Reproduction, mutation and crossover are the most common genetic operators, which can be described as follows. Reproduction operator selects a couple of parents that will produce the next generation. Parents with higher fitness have more chances for reproduction, but chance of being selected is also given to parents who have lower fitness conditions because they may have valuable genes. Crossover operator is applied to the two selected chromosomes so that they share their structure based on a specified probable value. This operation creates a pair of new chromosomes that includes characterization of their parents. After reproduction and crossover, mutation operator is applied to each of the produced chromosomes. When the above algorithm is applied to the problem under study, the following maximal mechanical properties for the optimal conditions were obtained: for the ultimate tensile strength, HIPS content of 4.54%, SiO₂ content of 4.15%, and hardener content of 28.6 phr. These optimal condition values for damping ratio in

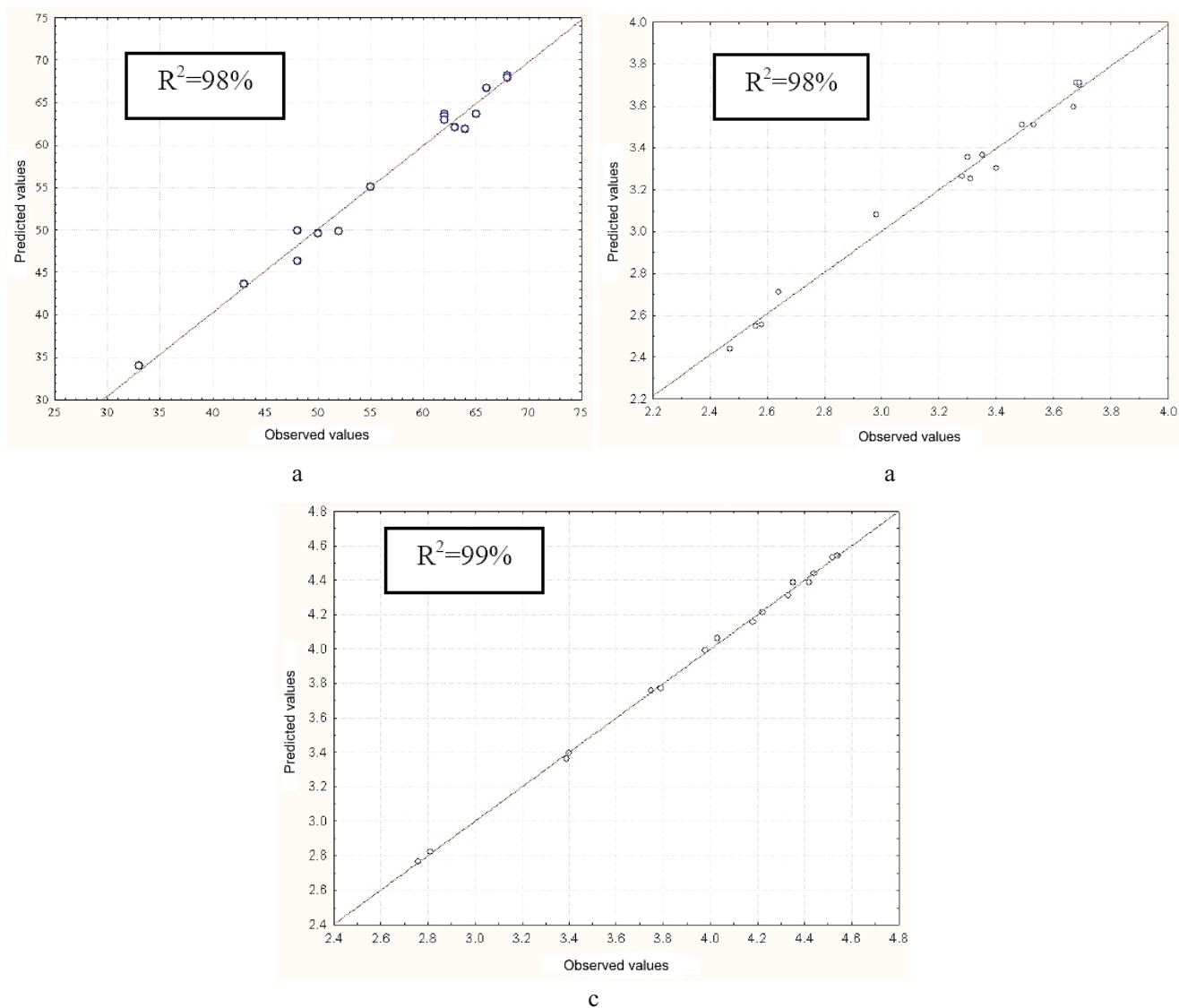


Fig. 4. Predicted vs observed data for tensile (a), damping ratio-first mode (b), and damping ratio-second mode (c).

the first mode are 4.87% for HIPS, 5.5% for nanosilica and 29.25 phr for hardener. Finally, the best concentrations of modifiers and hardener for damping ratio in the second mode are: 5.05% for HIPS, 5.51% for nanosilica, and 29.56% phr for hardener. The maximal values of mechanical properties predicted by the model at the optimal values of variables were as follows: 69.8 MPa for UTS, 3.79% for damping ratio in the first mode, and 4.67% for damping ratio in the second mode. Upon preparation of samples, according to the optimal conditions, they were tested, in order to provide verification of the predicted results. By using five replications for each experiment, the following average results have been obtained: 68.5 MPa for UTS, 3.75% for damping ratio in the first mode, and 4.61% for damping ratio in the second mode. Analysis of the results obtained shows that the experimental values have a close fit with those predicted by the model. Similar to results of previous studies, it was found that simultaneous addition of nano- and thermoplastic phases to epoxy resin results in higher toughness of the material. Mirmohseni and Zavareh [42] have shown that by adding 2% clay and 20% polyamide, the material toughness can be increased by 115%. Mirmohseni and Zavareh [43] demonstrated that with incorporation of 2.5% clay nanolayered and 4 phr ABS into epoxy matrix, 133% improvement was observed for impact strength.

Ultimate tensile strength of epoxy/HIPS/SiO₂

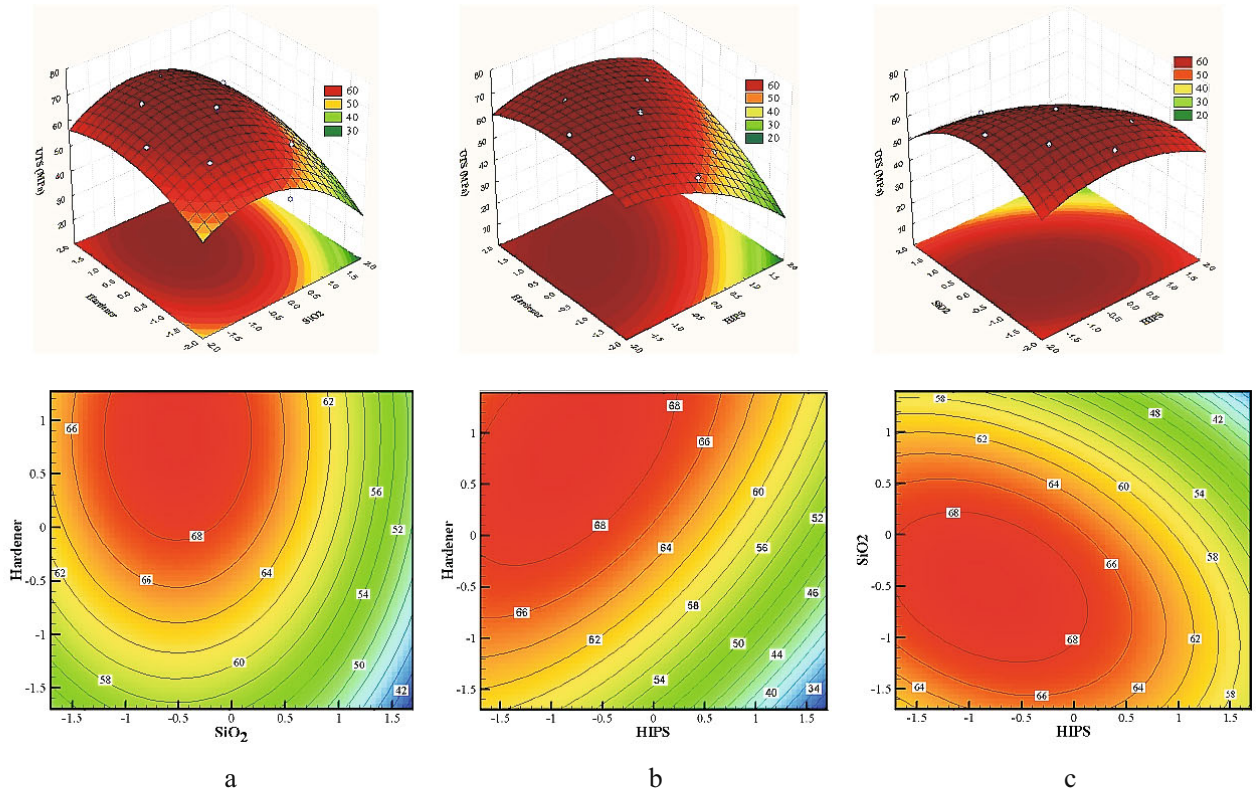


Fig. 5. 3D and contour plots of UTS at HIPS = -0.82 (a), SiO₂ = -0.5 (b), hardener = 0.87 (c).

Damping ratio-first mode of epoxy/HIPS/SiO₂

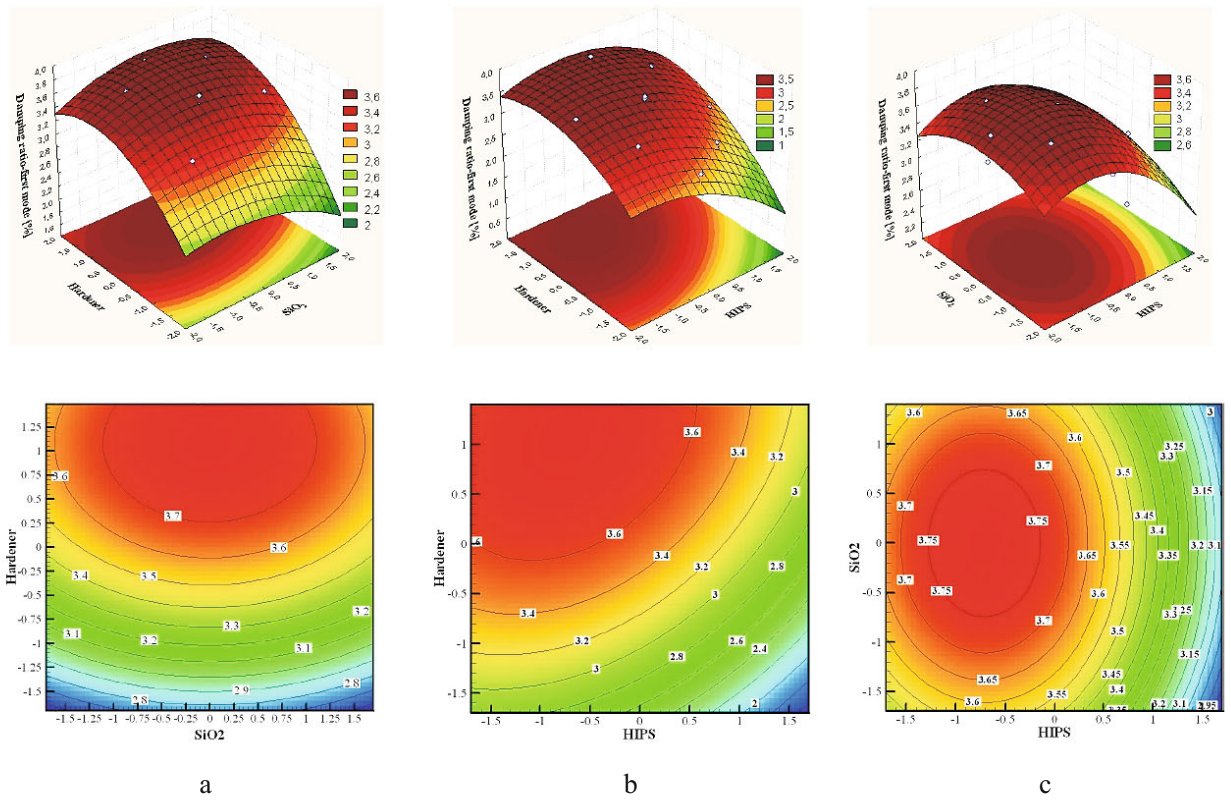


Fig. 6. 3D and contour plots of damping ratio-first mode at HIPS = -0.71 (a), SiO₂ = 0 (b), hardener = 1.09 (c).

Damping ratio-second mode of epoxy/HIPS/SiO₂

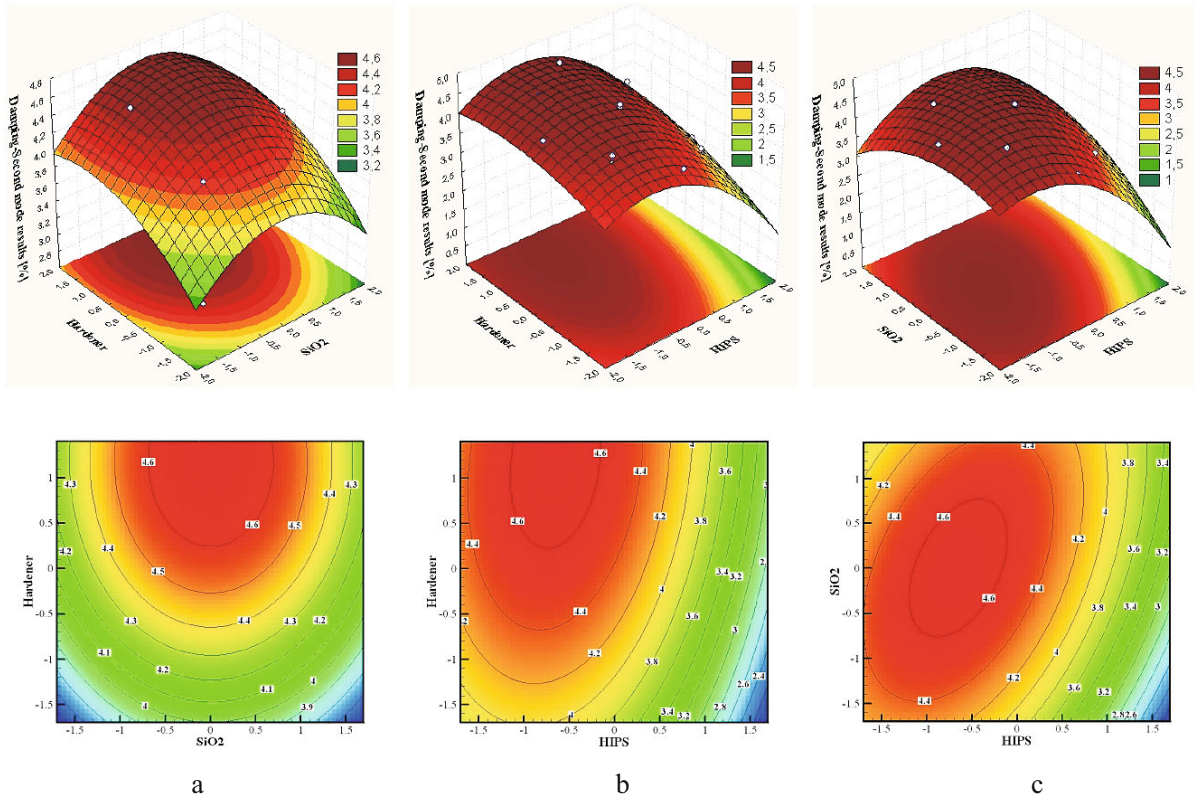
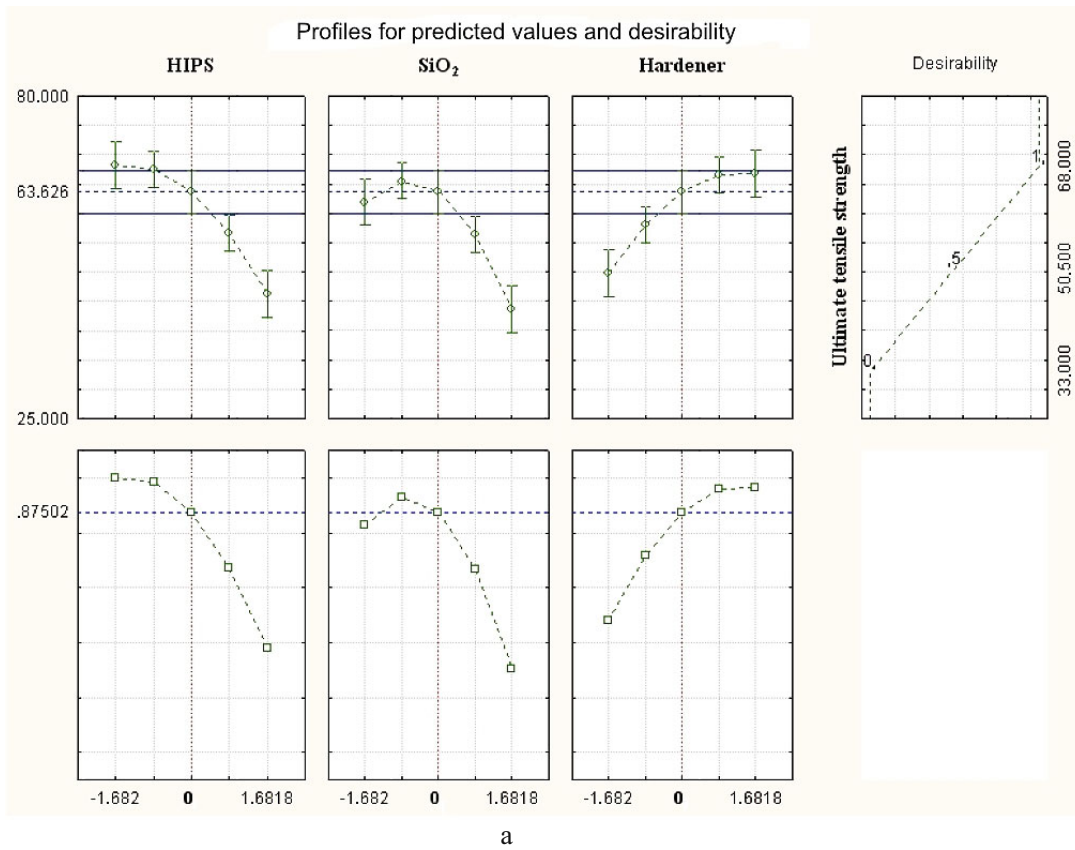


Fig. 7. 3D and contour plots of damping ratio-second mode at HIPS = -0.65 (a), SiO₂ = 0 (b), hardener = 1.19 (c).

Ultimate tensile strength of epoxy/HIPS/SiO₂



a

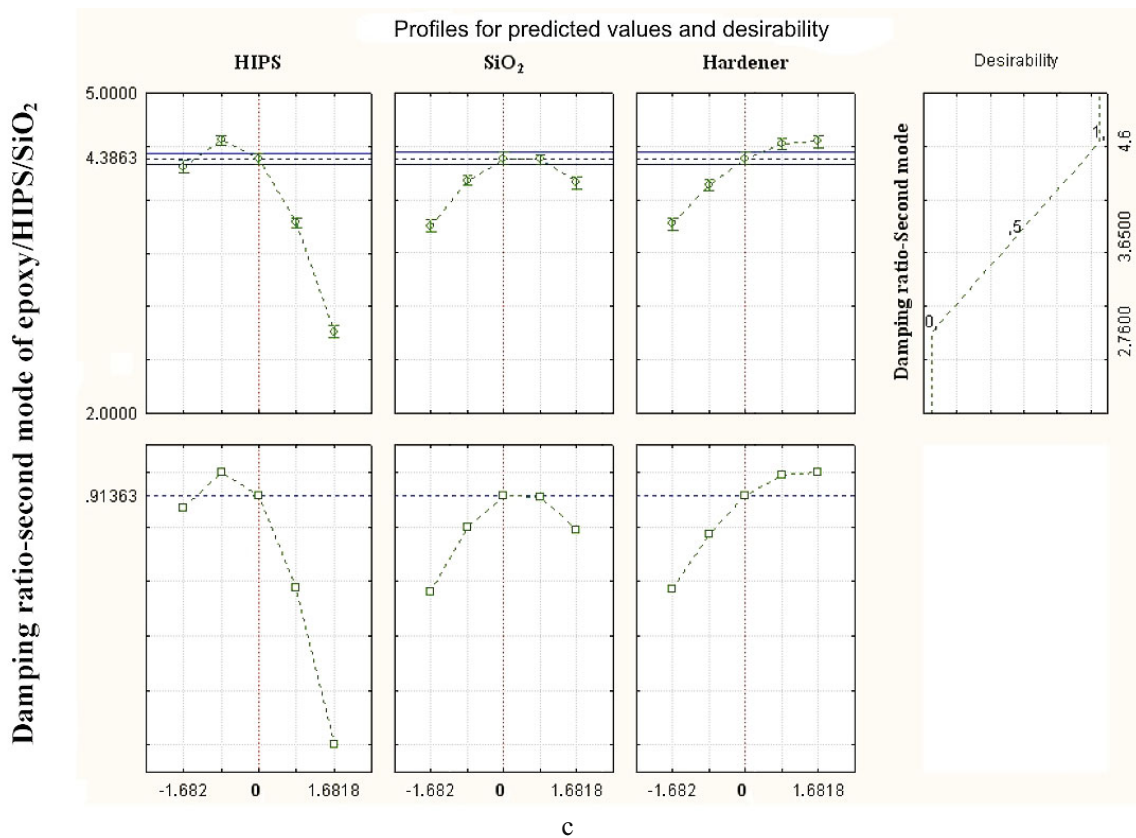
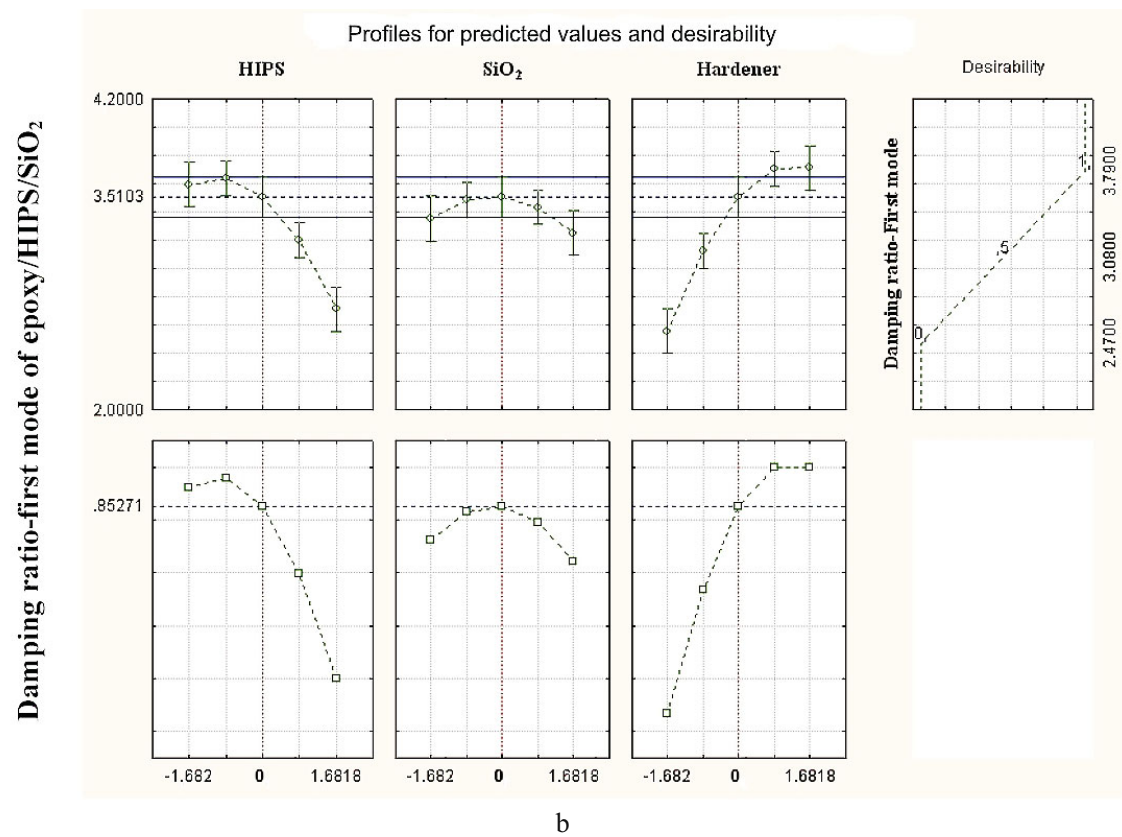


Fig. 8. Profiles for predicted values and desirability function for UTS (a), damping ratio-first mode (b), damping ratio-second mode (c).

2.3. 3D and Contour Plots for Mechanical Behavior of Epoxy-Based Hybrid Nanocomposite. In this study, in order to show the dependence of mechanical properties of epoxy-based hybrid nanocomposite on such effective parameters as design factors, the 3D response surface and contour plots are employed.

2.3.1. Effect of Hardener and Silica Loading on Mechanical Properties. Figures 5a, 6a, and 7a present 3D response surface and 2D contour plots of the ultimate tensile strength and damping ratio for the first and second modes of epoxy/ HIPS/SiO₂ ternary nanocomposite as a function of hardener and silica nanoparticles contents, while HIPS factor was at its optimal concentration for each property. As one can see from the results, in similar cases silica content and hardener loading have significant effects on the measured mechanical properties. The tensile and damping values in the first and second modes increased with increasing silica content to some extent and decreased with higher loading. This amount varied between 4.15–5.51%. As Mirmohseni and Zavareh reported in [43], the above figures indicate that the best concentration of hardener in hybrid mechanism does not correspond to stoichiometric ratio (23 phr), whereas the optimal loading for hardener occurs in the range of 28.40–29.56 phr. Also it can be concluded that hardener and silica nanoparticles provide no significant interaction effect on the results. A possible reason for these phenomena may be attributed to the fact that due to small size and low concentration of silica nanoparticles, these particles cannot inhibit the performance of hardener in polymerization of epoxy monomers.

2.3.2. Effect of Hardener and HIPS Loading on Mechanical Properties. Figures 5b, 6b, and 7b depict the response surface and contour plots, which demonstrate the effects of HIPS and hardener factors on the ultimate tensile strength, damping ratio for the first and second modes of epoxy/HIPS/silica hybrid nanocomposite, whereas the SiO₂ loading is fixed at its best concentration for each property. It is seen from the figures that the hardener behavior is similar to that described in the previous section. It seems that the main processing defects in epoxy-based nanocomposites are related to the entrained voids and incomplete cure during the cross-linking phase. Noteworthy is that HIPS loading yields the optimal mechanical strength values at different contents. The optimal amount of HIPS for tensile loading is 4.54%, for damping ratio at the first mode – 4.87% and finally, for damping ratio at the second mode – 5.05%. In these results, the main feature is a considerable interaction effect between HIPS and hardener for the ultimate tensile strength and lower interaction for damping ratios at the first and second modes, as compare to that in tensile mode. This behavior may be related to the large size of HIPS particles that inhibit complete involvement of epoxy monomers by hardener and reduce the chance of all epoxy monomers to participate in polymerization and network forming that lead topoor strength of epoxy. But insofar as rigidity is a negative parameter from the standpoint of damping properties, this interaction has a feeble effect on the latter.

2.3.3. Effect of HIPS and SiO₂ Loading on Mechanical Properties. The effect of HIPS and nano-SiO₂ contents upon mechanical strength of epoxy-based nanocomposite is depicted in Figs. 5c, 6c, and 7c. As it follows from the results, they are strongly affected by these factors. Increase in toughness by usage of thermoplastic particles results in the matrix shear bonding and matrix dilation from the plastic zone in front of the crack tip [8, 9, 44, 45], which provide the improvement of damping properties. A localized plastic zone during vibration can absorb these waves, limiting the high local stresses and thereby can reduce the probability of vibration growth. Also this strategy may ensure absorption of more energy than it would be required for the equivalent propagation in brittle materials. Noteworthy is that interaction between HIPS and SiO₂ affects the tensile and damping strength values at the second mode, whereas this interaction is not observed in case of damping at the first mode. This behavior may be attributed to the fact that simultaneous presence of HIPS and SiO₂ increases the viscosity and decreases the possibility of homogeneous mixture formation. This may lead to agglomeration of SiO₂ nanoparticles and formation of large particles, which cannot absorb the energy of vibration in the material.

The results obtained indicate that the ultimate tensile strength of epoxy/ HIPS/SiO₂ ternary nanocomposite is increased by 69% for the optimal levels of parameters. The damping ratio at the first mode, in comparison with neat epoxy sample, is enhanced by 42%, while damping ratio at the second mode can be increased by 91%. This result shows the synergistic effect of silica and HIPS modifiers on damping strength of hybrid nanocomposite. These results indicate that addition of rigid nanoparticles (silica) enhances tensile strength, whereas addition of HIPS, as a thermoplastic phase, improves the vibration-absorbing ability of composite. In general, it may be concluded that simultaneous addition of HIPS as a thermoplastic modifier and silica as a nanoparticulate material can considerably improve the mechanical and damping strength values concurrently. The micrograph depicting the fracture surface of

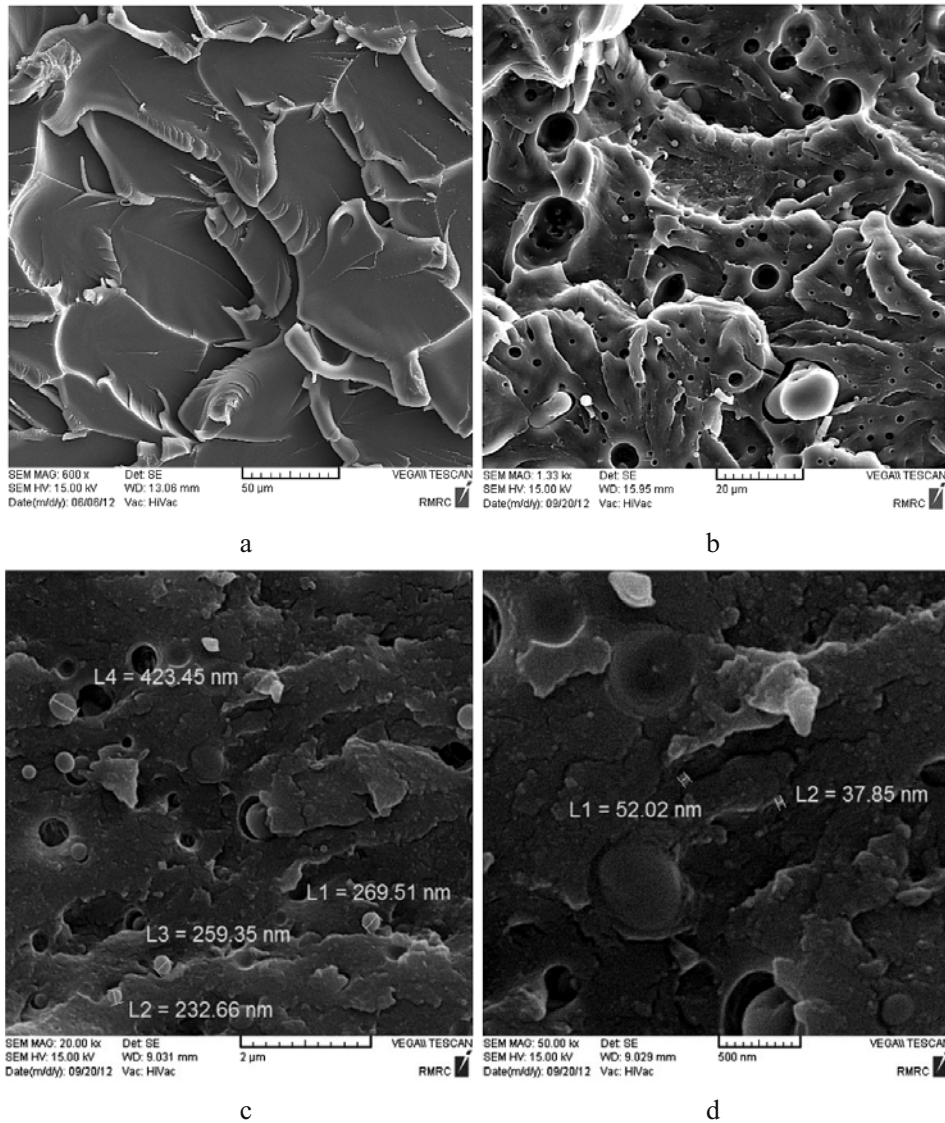


Fig. 9. Scanning electron micrographs of fracture surface for specimens: neat (a), with 3.5 wt.% SiO₂ and 4 wt.% HIPS (b, c, d).

tensile specimen with the optimal amount of HIPS, SiO₂ and hardener is shown in Fig. 9. In epoxy materials, cross-link density plays a vital role in achievement of good mechanical properties. As seen from Fig. 9, good dispersion of silica nanoparticles and high impact polystyrene as thermoplastic phase with small-scale agglomeration takes place. Moreover, phase separation of nano- and microparticles in epoxy-rich matrix is observed. Thus, modifier with homogenous dispersion can act as crack stopper and reinforcement, enhancing the mechanical strength [46, 47].

Conclusions. A new combination of thermoplastic-nanofiller as a modifier for epoxy-based composite is proposed. In this study, tensile and damping properties at the first and second modes have been investigated. The central composite model is applied for prediction and optimization of the results. A genetic algorithm is used to optimize the models provided by CCD. In addition, the effects of parameters on mechanical strength of epoxy/HIPS/SiO₂ ternary nanocomposite are described by 3D response surface and 2D contour plots. As follows from the results obtained, combination of HIPS and silica nanoparticles significantly increases the epoxy resin tensile strength, as well as damping properties for the first and second modes by 69, 42, and 91%, respectively. Correlation between morphology and mechanical properties is observed via the SEM technique.

REFERENCES

1. M. M. Shokrieh, M. A. Torabizadeh, and A. Fereidoon, "A new method for evaluation of mechanical properties of glass/epoxy composites at low temperatures," *Strength Mater.*, **44**, No. 1, 87–99 (2012).
2. M. M. Shokrieh, M. A. Torabizadeh, and A. Fereidoon, "Progressive failure analysis of glass/epoxy composites at low temperatures," *Strength Mater.*, **44**, No. 3, 314–324 (2012).
3. A. V. Buketov, P. D. Stukhlyak, V. V. Levyts'kyi, et al., "A study of creep of epoxy composites with continuous fibers and modified fine filler in aggressive media," *Strength Mater.*, **43**, No. 3, 338–346 (2011).
4. H. Kishi, M. Kuwata, S. Matsuda, et al., "Damping properties of thermoplastic-elastomer interleaved carbon fiber-reinforced epoxy composites," *Compos. Sci. Technol.*, **64**, 2517–2523 (2004).
5. A. J. Kinloch, M. L. Yuen, and S. D. Jenkins, "Thermoplastic-toughened epoxy polymers," *J. Mater. Sci.*, **29**, 3781–3790 (1994).
6. R. D. Brooker, A. J. Kinloch, and A. C. Taylor, "The morphology and fracture properties of thermoplastic-toughened epoxy polymers," *J. Adhes.*, **86**, Issue 7, 726–741 (2010).
7. E. H. Rowe, A. R. Siebert, and R. S. Drake, "Toughening thermosets with butadiene/acrylonitrile polymers," *Mod. Plast.*, **47**, 110–117 (1970).
8. A. J. Kinloch, S. J. Shaw, D. A. Tod, and D. L. Hunston, "Deformation and fracture behaviour of a rubber-toughened epoxy: 1. Microstructure and fracture studies," *Polymer*, **24**, Issue 10, 1341–1354 (1983).
9. R. A. Pearson and A. F. Yee, "Toughening mechanisms in elastomer-modified epoxies," *J. Mater. Sci.*, **21**, 2475–2488 (1986).
10. N. G. Yun, Y. G. Won, and S. C. Kim, "Toughening of epoxy composite by dispersing polysulfone particle to form morphology spectrum," *Polym. Bull.*, **52**, 365–372 (2004).
11. M. Kimoto and K. Mizutani, "Blends of thermoplastic polyimide with epoxy resin: Pt. II. Mechanical studies," *J. Mater. Sci.*, **32**, 2479–2483 (1997).
12. A. Mirmohseni and S. Zavareh, "Preparation and characterization of an epoxy nanocomposite toughened by a combination of thermoplastic, layered and particulate nano-fillers," *Mater. Des.*, **31**, No. 6, 2699–2706 (2010).
13. K. Mimura, H. Ito, and H. Fujioka, "Improvement of thermal and mechanical properties by control of morphologies in PES-modified epoxy resins," *Polymer*, **41**, Issue 12, 4451–4459 (2000).
14. L. R. F. Rose, "Toughening due to crack-front interaction with a second-phase dispersion," *Mech. Mater.*, **6**, Issue 1, 11–15 (1987).
15. K. T. Faber and A. G. Evans, "Crack deflection processes – II. Experiment," *Acta Metall.*, **31**, No. 4, 577–584 (1983).
16. J. Lee and A. F. Yee, "Inorganic particle toughening I: Micro-mechanical deformations in the fracture of glass bead filled epoxies," *Polymer*, **42**, No. 2, 577–588 (2001).
17. J. Lee and A. F. Yee, "Inorganic particle toughening II: Toughening mechanisms of glass bead filled epoxies," *Polymer*, **42**, No. 2, 589–597 (2001).
18. J. Lee and A. F. Yee, "Fracture of glass bead/epoxy composites: on micromechanical deformations," *Polymer*, **41**, Issue 23, 8363–8373 (2000).
19. T. Kawaguchi and R. A. Pearson, "The effect of particle–matrix adhesion on the mechanical behavior of glass filled epoxies. Pt. 2. A study on fracture toughness," *Polymer*, **44**, Issue 15, 4239–4247 (2003).
20. T. H. Hsieh, A. J. Kinloch, K. Masania, et al., "The mechanisms and mechanics of the toughening of epoxy polymers modified with silica nanoparticles," *Polymer*, **51**, Issue 26, 6284–6294 (2010).
21. C. Roscher, "Tiny particles, huge effect: Radiation curable silica nanocomposites for scratch and abrasion resistant coatings," *Eur. Coat. J.*, No. 4, 138–142 (2003).
22. R. A. Vaia, T. Benson Tolle, G. F. Schmitt, et al., "Nanoscience and nanotechnology: materials revolution for the 21st century," *SAMPE J.*, **37**, 4–31 (2001).
23. E. T. Thostenson, C. Li, and T.-W. Chou, "Nanocomposites in context," *Compos. Sci. Technol.*, **65**, 491–516 (2005).

24. B. Wetzel, F. Hauptert, K. Friedrich, et al., "Impact and wear resistance of polymer nanocomposites at low filler content," *Polymer Eng. Sci.*, **42**, Issue 9, 1919–1927 (2002).
25. H. Zou, S. Wu, and J. Shen, "Polymer/silica nanocomposites: preparation, characterization, properties, and applications," *Chem. Rev.*, **108**, 3893–3957 (2008).
26. A. Asif, K. Leena, V. Lakshmana Rao, and K. N. Ninan, "Hydroxyl terminated poly(ether ether ketone) with pendant methyl group-toughened epoxy clay ternary nanocomposites: preparation, morphology, and thermomechanical properties," *J. Appl. Polymer Sci.*, **106**, Issue 5, 2936–2946 (2007).
27. H. Zhang, L. A. Berglund, "Deformation and fracture of glass bead/CTBN-rubber/epoxy composites," *Polymer Eng. Sci.*, **33**, Issue 2, 100–107 (1993).
28. J. Lee and A. F. Yee, "Micro-mechanical deformation mechanisms in the fracture of hybrid-particulate composites based on glass beads, rubber and epoxies," *Polymer Eng. Sci.*, **40**, Issue 12, 2457–2470 (2000).
29. F. Ravari, A. Omrani, A. A. Rostami, and M. Ehsani, "Ageing effects on electrical, morphological, and mechanical properties of a low viscosity epoxy nanocomposite," *Polymer Degrad. Stab.*, **97**, No. 6, 929–935 (2012).
30. A. Omrani, L. C. Simon, A. A. Rostami, and M. Ghaemy, "Cure kinetics, dynamic mechanical and morphological properties of epoxy resin–Im6NiBr2 system," *Eur. Polymer J.*, **44**, No. 3, 769–779 (2008).
31. A. Omrani, L.C. Simon, and A. A. Rostami, "Influences of cellulose nanofiber on the epoxy network formation," *Mater. Sci. Eng. A*, **490**, 131–137 (2008).
32. R. Leardi, "Experimental design in chemistry: a tutorial," *Anal. Chim. Acta*, **652**, 161–172 (2009).
33. P. Angelopoulos, H. Evangelaras, and C. Koukouvinos, "Small, balanced, efficient and near rotatable central composite designs," *J. Statist. Plan. Infer.*, **139**, No. 6, 2010–2013 (2009).
34. J. S. Chung and S. M. Hwang, "Application of a genetic algorithm to the optimal design of the die shape in extrusion," *J. Mater. Process. Technol.*, **72**, No. 1, 69–77 (1997).
35. R. G. Song and Q. Z. Zhang, "Heat treatment optimization for 7175 aluminum alloy by genetic algorithm," *Mater. Sci. Eng. C*, **17**, Issues 1-2, 133–137 (2001).
36. R.-G. Song, Q.-Z. Zhang, M.-K. Tseng, and B.-J. Zhang, "The application of artificial neural networks to the investigation of aging dynamics in 7175 aluminium alloys," *Mater. Sci. Eng. C*, **3**, Issue 1, 39–41 (1995).
37. P. van Overschee and B. de Moor, *Subspace Identification for Linear Systems. Theory–Implementation–Applications*, Kluwer Academic Publishers, Dordrecht (1996).
38. B. Peeters, *System Identification and Damage Detection in Civil Engineering*, Ph.D. Thesis, Katholieke Universiteit Leuven, Belgium (2000).
39. A. R. Brincker and P. Andersen, "Understanding stochastic subspace identification," in: Proc. of International Modal Analysis Conference (IMAC), Denmark (2006), pp. 461–466.
40. E. Morgan (Ed.), *Chemometrics: Experimental Design*, Wiley, Chichester (1995).
41. M. Hadjmohammadi and V. Sharifi, "Simultaneous optimization of the resolution and analysis time of flavonoids in reverse phase liquid chromatography using Derringer's desirability function," *J. Chromatogr. B*, **880**, 34–41 (2012).
42. A. Mirmohseni and S. Zavareh, "Modeling and optimization of a new impact-toughened epoxy nanocomposite using response surface methodology," *J. Polymer Res.*, **18**, 509–517 (2011).
43. A. Mirmohseni and S. Zavareh, "Epoxy/acrylonitrile-butadiene-styrene copolymer/clay ternary nanocomposite as impact toughened epoxy," *J. Polymer Res.*, **17**, No. 2, 191–201 (2010).
44. Y. Huang and A. J. Kinloch, "Modelling of the toughening mechanisms in rubber-modified epoxy polymers," *J. Mater. Sci.*, **27**, Issue 10, 2763–2769 (1992).
45. A. F. Yee and R. A. Pearson, "Toughening mechanisms in elastomer-modified epoxies," *J. Mater. Sci.*, **21**, 2462–2474 (1986).
46. J. López, C. Ramirez, M. J. Abad, et al., "Blends of acrylonitrile–butadiene–styrene with an epoxy/cycloaliphatic amine resin: phase-separation behavior and morphologies," *J. Appl. Polymer Sci.*, **85**, Issue 6, 1277–1286 (2002).
47. Y. Müller, L. Häußler, and J. Pionteck, "ABS-modified epoxy resins – curing kinetics, polymerization induced phase separation, and resulting morphologies," *Macromolec. Symp.*, **254**, Issue 1, 267–273 (2007).